Original Research

Perfusion-Weighted MRI in Evaluating the Intranodular Hemodynamic Characteristics of Dysplastic Nodules and Hepatocellular Carcinomas in an Experimental Rat Model

Hui Xu, PhD,[1] Jing-Xia Xie, MD,[1] Xuan Li, MD,[1]* Zheng-Han Yang, MD,[2] Zhuo-Zhao Zheng, MD,[1] Bin Wang, MD,[3] and Zheng Wang, MD[4]

Purpose: To investigate the value of perfusion-weighted MRI in the evaluation of the intranodular hemodynamic characteristics of dysplastic nodules (DNs) and hepatocellular carcinomas (HCCs) in an experimental rat model.

Materials and Methods: A total of 40 rats with chemically-induced DNs and HCCs were investigated. Single-slice gadolinium-enhanced perfusion-weighted MRI was performed to evaluate the nodules. Time to peak (Tp), maximal relative signal enhancement (REmax), and the initial slope of signal intensity (SI) vs. time curves of the nodules and cirrhotic liver were evaluated. Nodules precisely corresponding to MRI were examined histologically. Paired Student's t-tests were used to compare the difference between nodules and cirrhotic liver.

Results: A total of 20 HCCs and 14 DNs were evaluated. HCCs showed a significantly higher REmax, shorter Tp, and higher slope than adjacent cirrhotic liver. The REmax and slope of DNs were significantly lower than adjacent cirrhotic liver parenchyma. Although the Tp of DNs was delayed two to three seconds compared to adjacent cirrhotic liver, there was no significant difference between them.

Conclusion: Perfusion-weighted MRI detected the intranodular hemodynamic characteristics of DNs and HCCs in an experimental rat model. DNs were hypovascular compared to cirrhotic liver, while HCCs were markedly hypervascular.

Key Words: magnetic resonance imaging; diffusion; hepatocellular carcinoma; dysplastic nodule; animal model
J. Magn. Reson. Imaging 2008;27:102–109.

HEPATOCELLULAR CARCINOMAS (HCCs) are the most common primary malignant tumors of the liver, with highest incidences occurring in Africa, Southeast Asia, and China (1). Western hemisphere incidences have increased in the last two decades as a result of viral diseases such as hepatitis B and C, and by excessive alcohol consumption (1–3). Cirrhotic liver is often the background from which HCCs arise. Many HCCs develop through a progressive pathway from a benign regenerative nodule to a dysplastic nodule (DN) to a DN with microscopic foci of an HCC, which may enlarge and replace the nodule, giving rise to a small HCC, and finally to the overt HCC in cirrhotic liver (4–10). At present, small HCCs are usually treated with resection or with liver transplantation (11). Therefore, it is important clinically to detect DNs and HCCs at an early stage to improve patient outcome and decision-making regarding therapeutic strategies.

In the multistep process of hepatocarcinogenesis, hepatocellular nodules demonstrate varying degrees of cytological and architectural atypia. In addition, accompanying the malignant evolution of hepatic nodules is a gradual change in blood supply from portal to arterial (12,13). This change in intranodular blood supply offers an opportunity for the radiological differentiation of benign and malignant lesions. Imaging techniques such as computed tomography hepatic arteriography (CTHA), computed tomography (CT) arterial portography (CTAP), dual- and triple-phase helical CT, contrast-enhanced dynamic MRI with non-liver-specific gadolinium-chelate, color Doppler, and contrast-enhanced sonography have been developed for nodule detection and characterization. Among those methods, CTAP and CTHA have been used successfully to detect the change of blood supply from portal to arterial during the course of malignant transformation

[1]Department of Radiology, Peking University Third Hospital, Beijing, China.
[2]Department of Radiology, Beijing Hospital, Beijing, China.
[3]Department of Radiology, Affiliated Hospital, Weifang Medical University, Weifang, China.
[4]Department of Pathology, Beijing Hospital, Beijing, China.
Contract grant sponsor: Nature and Science Foundation of Beijing; Contract grant number: 7063091.
*Address reprint requests to: X.L. and Jing-Xia Xie, Dept. of Radiology, Peking University Third Hospital, 49 North Garden Road, Haidian District, Beijing 100083, P.R. China. E-mail: mrhepatic@yahoo.com.cn
Received October 18, 2006; Accepted August 29, 2007.
DOI 10.1002/jmri.21188
Published online 16 November 2007 in Wiley InterScience (www.interscience.wiley.com).

of hepatic nodules. It should be noted that CTAP and CTHA are both invasive and costly, with significant rates of false-positive results and no substantial increase in sensitivity.

Perfusion-weighted MRI is a noninvasive technique for measuring parameters related to parenchyma perfusion and permeability. It has been used to assess angiogenesis and perfusion changes in tumors after antiangiogenic agent administration (14). To our knowledge, very few studies (15) have examined the use of perfusion-weighted MRI to assess the blood supply of DNs. The purpose of this study was to investigate the value of perfusion-weighted MRI in the evaluation of the intranodular hemodynamic characteristics of DNs and HCCs in an experimental HCC rat model.

MATERIALS AND METHODS

Animal Model

The experiment was performed in accordance with the Guide for the Care and Use of Laboratory Animals published by the U.S. National Institutes of Health (NIH Publication No. 85-23, revised 1996), with the approval of the local ethical committee for animal care and use. Six-week-old male Sprague-Dawley rats ($N = 40$) weighing 120–150 g were supplied by the Department of Laboratory Animal Science, Peking University, China. The animals were acclimated for one week and maintained under specific pathogen-free (SPF) environmental conditions with lighting from 09:00 to 21:00, temperature at 22 ± 2°C, and relative humidity at 45% to 60%. They were fed chow pellets and solution ad libitum during the entire study period.

HCCs were induced using 70 mg/kg diethylnitrosamine (DEN; 0.95 g/mL, Sigma Chemical Co., USA) intragastrically once a week for 10 weeks according to a treatment protocol modified from Fournier et al (16) and other researchers (17,18). The histological features of the hepatic nodules in this model simulate the type of lesions observed in human cirrhotic liver carcinogenesis (16–18).

MRI

From week 10 to week 20 after DEN treatment, three to four treated animals were randomly scanned every week. Before imaging, rats fasted for 12 hours and were anesthetized with 40 mg/kg pentobarbital sodium (Nembutal; Beijing Chemical Co., Beijing, China) intraperitoneally. The rats were examined with a 1.5T whole-body Sonata MR system (Siemens, Erlangen, Germany) with a maximum gradient capability of 40 mT/m. A two-channel phased-array coil (50 mm in diameter; Chen Guang Medical Science Co., Shanghai, China) for animals was used to obtain all MR images. Rats were placed inside the coil in the supine position and the abdomen was fixed to prevent movement.

To detect hepatic nodules, conventional liver MR protocols were used as follows: T2-weighted turbo spin-echo transverse, sagittal, and coronal orientation sequences with fat saturation (TR = 3000 msec, TE = 79 msec, flip angle = 150°, echo train length = 7, average = six times, field of view = 90 mm × 65 mm, matrix size = 192 × 135, slice thickness = 3 mm, and intersection gap = 0.3 mm), transverse two-dimensional T1-weighted fast low-angle shot (FLASH) sequence with fat saturation (TR = 250 msec, TE = 3.53 msec, flip angle = 70°, average = four times, field of view = 90 mm × 55 mm, matrix size = 192 × 135, slice thickness = 3 mm, and intersection gap = 0.3 mm).

Dynamic contrast-enhanced MRI was used to monitor the first pass of gadolinium diethylene triaminepenta acetate (Gd-DTPA) (Magnevist; Schering AG, Berlin, Germany) through the nodule with a single-slice inversion-recovery two-dimensional turbo-FLASH sequence (TR = 500 msec, TE = 2.75 msec, TI = 160 msec, flip angle = 10°, field of view = 80 mm × 50 mm, matrix size = 128 × 100, slice thickness = 3.5 mm, average = two times), resulting in a temporal resolution of one second. After the tenth image was obtained, Gd-DTPA was rapidly administered manually (at a rate of approximately 0.5 mL/second following 0.5 mL of saline flush) by one investigator via the tail vein of the rat at a dose of 0.1 mmol Gd/kg. This sequence was applied continuously for 120 measurements.

There were multiple nodules in the liver of several rats, so these were scanned two to four times each. From the first scan to the last, there were fewer than three to four days. Immediately after the last MRI session, the rats were sacrificed for pathologic examination.

Histology

Each animal was sacrificed after completing MRI. The liver was removed and cut sequentially into 3-mm sections in the transverse plane that corresponded as closely as possible to the MRI plane. The nodules that precisely corresponded to perfusion-weighted MRI (using the transverse, sagittal, and coronal orientations of T2-weighted images as a reference) were determined. These were then fixed in 4% buffered formalin, embedded in paraffin, and thinner 5-μm sections were cut and stained with hematoxylin-eosin for histological examination. Histological examination was conducted by two hepatopathologists with at least 10 years of experience in liver pathology and a consensus was achieved. Using the diagnostic criteria from the International Working Party's "Terminology of Nodular Hepatocellular Lesions" (4), nodules were classified as low-grade dysplastic nodules (LGDN), high-grade dysplastic nodules (HGDN), well-differentiated HCC (HCCwell), moderately-differentiated HCC (HCCmod), or poorly-differentiated HCC (HCCpoor).

Data Analysis

Perfusion-weighted MR images were analyzed using commercially available software (Mean Curve; Siemens Medical Systems) on the MR unit. Regions of interest (ROIs) were placed where the nodules had been observed on corresponding pathological slices. We also placed ROIs on liver parenchyma that presented cirrhotic liver tissue on pathological examination. Signal intensities (SIs) were measured for each MR image. SI results were plotted as a function of time, and SI vs. time (SI-T) curves were obtained.

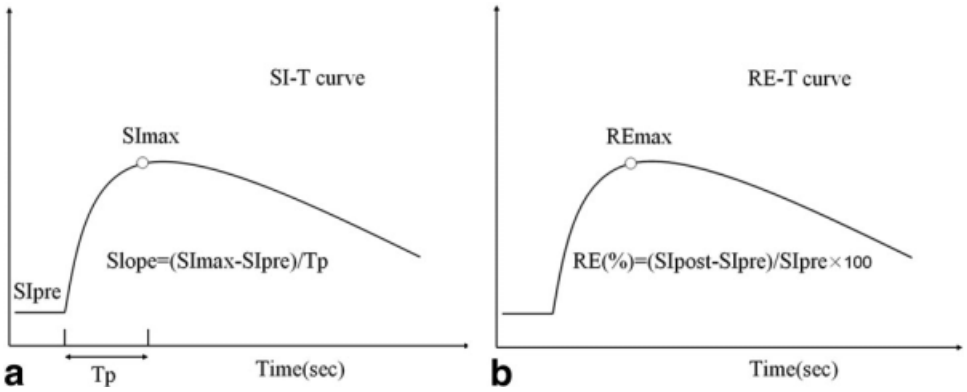

Figure 1. a: SI-T curve. **b:** RE-T curve. Three parameters: SIpre in SI-T curve = SI before the injection of contrast, SImax = maximal SI value in the SI-T curve, Tp = time interval between SIpre and SImax.

The relative signal enhancement (RE) of each nodule and its adjacent tumor-free region were calculated using the equation RE(%) = [(SIpost − SIpre)/SIpre] × 100, where SIpre and SIpost are the signal intensities before and after injection of Gd-DTPA. RE-T (relative signal enhancement vs. time) curves of hepatic nodules and adjacent cirrhotic liver were obtained. In addition, the maximal relative signal enhancement (REmax) was evaluated for each ROI.

For quantitative assessment of the perfusion parameters of nodules and adjacent cirrhotic liver, time to peak (Tp), REmax, and the initial slope of SI-T curves were estimated (Fig. 1). The slope was calculated as (SImax − SIpre)/Tp, where SImax is the peak SI value in the SI-T curve.

Statistical Analysis

All data are expressed as mean ± SD. Paired Student's *t*-tests were used to compare nodular lesions and adjacent cirrhotic liver. Data analyses were performed on a personal computer using statistical software (SPSS for windows, version 12; SPSS Inc, Chicago, IL, USA). A two-tailed *P* value of less than 0.05 was required for statistical significance.

RESULTS

Out of 40 rats presenting tumors, seven died spontaneously of their disease before we could complete the study and four died as a result of anesthesia during imaging. Therefore, 29 rats completed the protocol.

Based on precisely correlating nodular lesions in the resected liver with the location of nodular lesions visualized with MR, a total of 34 nodules were found in 25 of the 29 rats. Among these, 14 DNs (eight LGDNs and six HGDNs) were identified in 12 rats, with diameters ranging from 3 mm to 7 mm (mean = 4 mm). A total of 20 HCCs (five HCCwell, nine HCCmod, and six HCCpoor) were found in 16 rats, with diameters ranging from 3 mm to 15 mm (mean = 7.1 mm).

The differences between perfusion parameters in hepatic nodules and adjacent cirrhotic liver are shown in Tables 1 and 2. In the 20 nodular HCCs, two RE-T curve patterns were found. Pattern 1, apparent in 14 HCCs (five HCCwell, six HCCmod, and three HCCpoor), showed a rapid wash-in and rapid wash-out pattern (Fig. 2). Pattern 2, apparent in six HCCs (three HCCmod and three HCCpoor), showed a rapid wash-in and slow wash-out pattern (Fig. 3). The REmax of HCCs was significantly higher than cirrhotic liver ($P < 0.001$). The Tp of HCCs was shorter than cirrhotic liver ($P < 0.001$) and the SI slope of HCCs was significantly higher than cirrhotic liver ($P < 0.001$).

Among the 14 DNs, three RE-T curve patterns were observed. Pattern 1, apparent in four LGDNs, showed the same RE-T curve, Tp, and REmax as adjacent cirrhotic liver, indicating a similar blood supply to the adjacent liver. Pattern 2, apparent in the RE-T curves of seven DNs (two LGNDs and five HGDNs; Fig. 4), was similar to that of adjacent cirrhotic liver, with nearly the same Tp, but the REmax of DNs was lower than adjacent liver. A third RE-T curve pattern (Fig. 5) was seen in three DNs (two LGDNs and one HGDN), and showed a slow increase in SI and maximal enhancement during the portal phase or later, followed by a plateau, and a REmax lower than adjacent cirrhotic liver. The latter two patterns of RE-T curves showed hypovascularity compared to adjacent cirrhotic liver characteristic of DNs. The REmax of DNs was lower than cirrhotic liver ($P < 0.001$). Although the Tp of DNs was delayed one to two seconds compared to cirrhotic liver, there was no significant difference between them ($P = 0.077$). The slope of DNs was significantly lower than cirrhotic liver ($P = 0.002$).

DISCUSSION

Blood supply to the various nodules in cirrhotic liver is complex. During the development of hepatocarcinogenesis, the intranodular portal supply tends to decrease and the intranodular hepatic arterial supply tends to increase (12,13,19). Recent histopathologic and immunohistochemical studies (20–23) showed that the de-

Table 1
Comparisons of Perfusion Parameters in HCCs and Adjacent Cirrhotic Liver Parenchyma*

	HCC ($N = 20$)	Cirrhotic liver ($N = 20$)	t	P
REmax	84.67 ± 22.15	59.46 ± 11.30	5.126	<0.001
Tp	8.70 ± 2.85	13.15 ± 2.18	−5.899	<0.001
Slope	9.21 ± 3.29	4.99 ± 1.13	5.580	<0.001

*Data are mean ± SD.

Table 2
Comparison of Perfusion Parameters in DNs and Adjacent Cirrhotic Liver Parenchyma*

	DN (N = 14)	Cirrhotic liver (N = 14)	t	P
REmax	51.46 ± 14.06	62.59 ± 13.57	−3.981	0.002
Tp	14.5 ± 4.11	12.78 ± 2.01	1.922	0.077
Slope	4.33 ± 1.49	5.12 ± 1.04	−4.013	0.002

*Data are mean ± SD.

gree of capillarization of sinusoids and the number of unpaired arteries (arteries not accompanied by bile ducts—considered neovascularized arteries) are related to the gradual change in blood supply from portal to arterial, as a DN becomes an HCC.

Our results demonstrate that HCCs show specific differences in perfusion parameters compared to adjacent cirrhotic liver parenchyma. Maximal enhancement of HCCs was found during the arterial phase, when the REmax and the initial slope of the SI-T curve were significantly higher than adjacent cirrhotic liver parenchyma. The results indicate that HCCs showed increased blood supply and were predominantly supplied by hepatic arteries. We observed a rapid increase in the enhancement of 14 HCC lesions during the hepatic arterial phase followed by a rapid wash-out of contrast material, which is considered a typical finding in HCCs (24,25). However, six moderately and poorly differentiated HCC lesions showed a rapid wash-in followed by a slow and progressive decrease. The difference between the two patterns of RE-T curves possibly relates to the pathology of HCCs. Moderately and poorly differentiated HCCs, because of increased extracellular space, would induce slow contrast wash-out. In addition, both necrosis and hemorrhage were common in moderately and poorly differentiated HCCs. Because the ROI in this study was the entire area of HCC nodules, that would also help explain the rapid wash-in but slow wash-out pattern of those six HCCs.

Several researchers (13,26,27) have evaluated the blood supply of DNs with CTHA and CTAP. They found that DNs are iso- or hypoattenuating with CTAP and CTHA relative to adjacent regenerative nodules, indicating that DNs have normal or slightly decreased portal and hepatic arterial supplies even though intranodular angiogenesis has already begun (21,23). Our study is consistent with their results. In addition, it is well known (28) that some well-differentiated HCCs are hypovascular.

Tajima et al (27) point out that the degeneration or disappearance of preexisting hepatic arteries causes a decline in intranodular arterial blood flow in DNs or well-differentiated HCCs. Insufficient growth of neovascularized arteries coupled with the disappearance of preexisting hepatic arteries results in hypovascularity compared with the surrounding hepatic parenchyma. As a result of a marked increase in neovascularized arteries, neovascular blood flow becomes dominant. The portal blood supply decreases with advancement of the tumor, and eventually, the tumor is fed mainly by arterial flow.

We believe that the hypothesis of Tajima et al (27) can explain the three different patterns of DN RE-T curves in our study. Four nodules, all LGDNs, had the same RE-T curve as adjacent cirrhotic liver. If preexisting hepatic arteries and portal veins have not yet decreased, LGDNs would have the same blood supply as

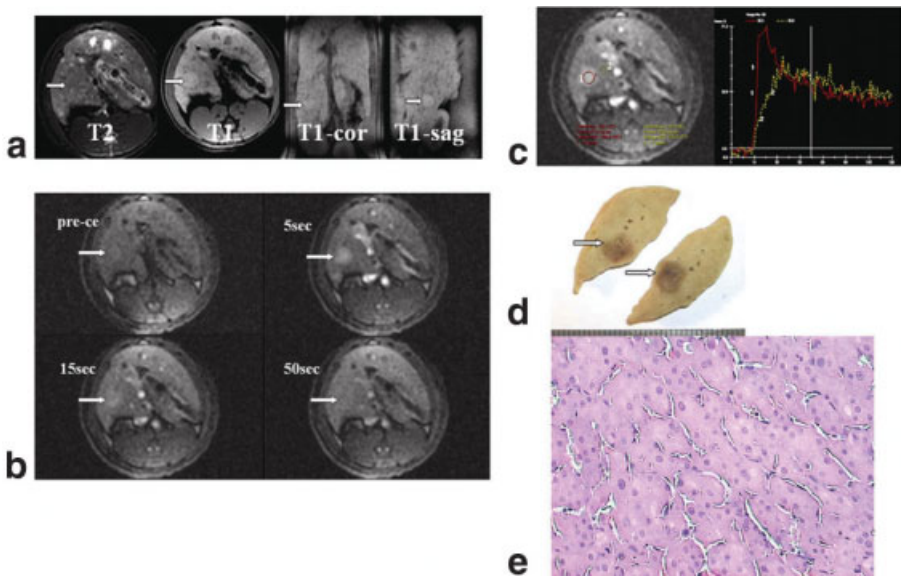

Figure 2. Well-differentiated HCC. **a:** Transverse, coronal, and sagittal FLASH fat-saturated T1-weighted MR images (TR/TE = 250 msec/3.53 msec; flip angle 70°) show a hyperintense nodule (arrow). In turbo spin-echo fat-saturated T2-weighted MR images (TR/TE = 3000 msec/79 msec, flip angle 150°), the HCC is isointense relative to adjacent liver tissue. **b:** Perfusion-weighted MR images (TR/TE = 500 msec/2.75 msec, flip angle 10°) of an HCC before and different times after injection of Gd-DTPA. **c:** The RE-T curve pattern of rapid wash-in and rapid wash-out. **d:** Corresponding transverse sections from the liver display the nodule (arrow). **e:** Photomicrography reveals a well-differentiated HCC (hematoxylin-eosin [H-E] stain, original magnification = ×400). [Color figure can be viewed in the online issue, which is available at www.interscience.wiley.com.]

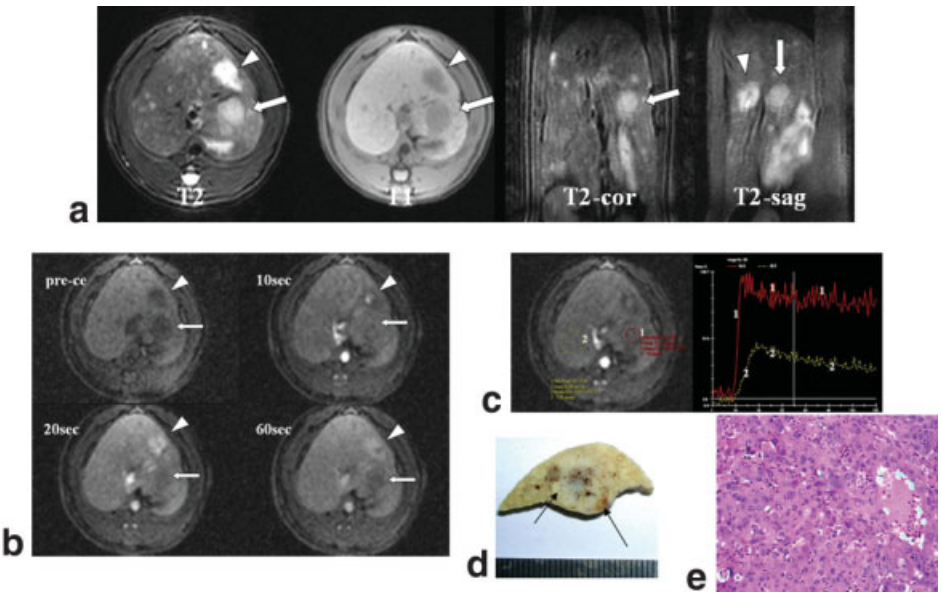

Figure 3. Poorly-differentiated HCC. **a:** Transverse, coronal, and sagittal turbo spin-echo fat-saturated T2-weighted MR images (TR/TE = 3000 msec/79 msec, flip angle = 150°) show a hyperintense nodule (arrow). In FLASH fat-saturated T1-weighted MR images (TR/TE = 250 msec/3.53 msec, flip angle = 70°), the HCC is hypointense. Another lesion (arrowhead) is a hemangioma. **b:** Perfusion-weighted MR images (TR/TE = 500 msec/2.75 msec, flip angle = 10°) of an HCC before and different times after injection of Gd-DTPA. **c:** The RE-T curve pattern of rapid wash-in and slow wash-out. **d:** Corresponding transverse sections from the liver display the tumor (black arrow). **e:** Histologic examination reveals poorly differentiated HCC (hematoxylin-eosin [H-E] stain, original magnification = ×400). [Color figure can be viewed in the online issue, which is available at www.interscience.wiley.com.]

the surrounding cirrhotic liver. Pattern 2 of the DN RE-T curves, seen in five HGDNs and two LGDNs, shows a rapid increase but the REmax was lower than cirrhotic liver. This hemodynamic state suggests that preexisting hepatic arteries and portal veins have decreased, and neovascularized arteries have developed, but are still insufficient. The third pattern of DN RE-T curves, seen in one HGDN and two LGDNs, shows a

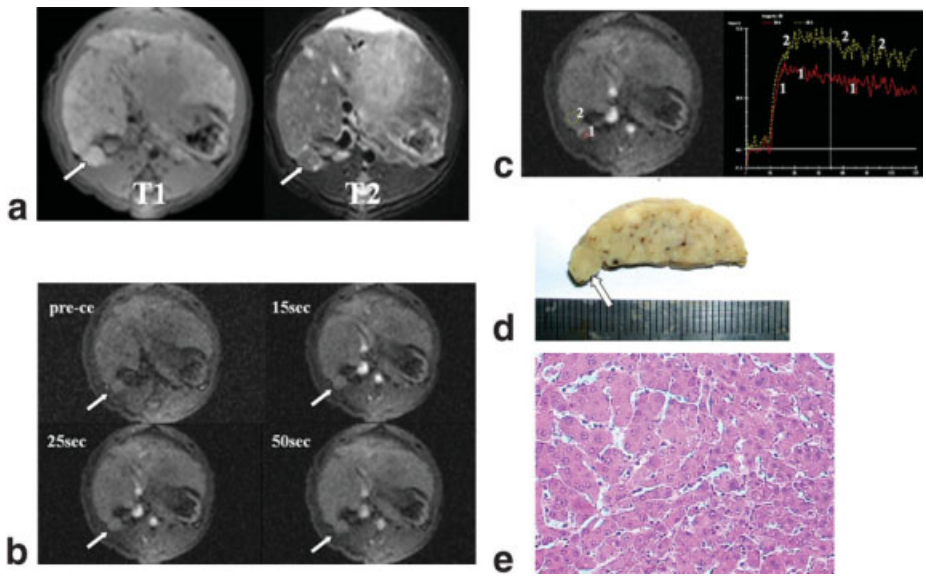

Figure 4. High-grade DN. **a:** Transverse turbo spin-echo fat-saturated T2-weighted MR image (TR/TE = 3000 msec/79 msec, flip angle = 150°) shows an isointense nodule (arrow). In a FLASH fat-saturated T1-weighted MR image (TR/TE = 250 msec/3.53 msec; flip angle = 70°), the DN is slightly hyperintense. **b:** Perfusion-weighted MR images (TR/TE = 500 msec/2.75 msec, flip angle = 10°) of the DN before and different times after injection of Gd-DTPA. **c:** The RE-T curve of the DN and adjacent cirrhotic liver parenchyma. The REmax of the DN was significantly lower than adjacent cirrhotic liver. **d:** Corresponding transverse sections from the liver display the nodule (arrow). **e:** The nodule was pathologically proved to be a high-grade DN (hematoxylin-eosin [H-E] stain, original magnification = ×400). [Color figure can be viewed in the online issue, which is available at www.interscience.wiley.com.]

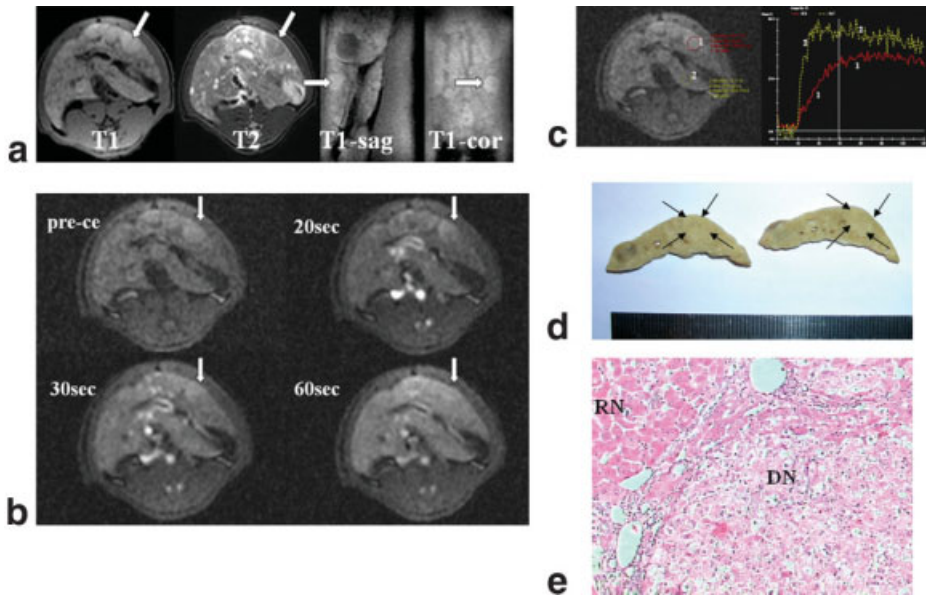

Figure 5. Low-grade DN. **a:** Transverse, coronal, and sagittal FLASH fat-saturated T1-weighted MR images (TR/TE = 250 msec/3.53 msec, flip angle = 70°) show a hyperintense nodule (arrow). In a turbo spin-echo fat-saturated T2-weighted MR image (TR/TE = 3000 msec/79 msec, flip angle = 150°), the DN is hypointense (arrow). **b:** Perfusion-weighted MR images (TR/TE = 500 msec/2.75 msec, flip angle = 10°) of the DN before and different times after injection of Gd-DTPA. **c:** The RE-T curve of the DN and adjacent cirrhotic liver. The RE-T curve of the DN showed a slow increase in SI at the arterial phase and maximal enhancement occurred during the portal phase, followed by a plateau. The REmax of the DN was significantly lower than adjacent cirrhotic liver. **d:** Resected specimen of the liver displays the nodule (black arrow). **e:** Histologic examination results revealed a low-grade DN (hematoxylin-eosin [H-E] stain, original magnification = ×200) and adjacent regenerative nodule (RN). [Color figure can be viewed in the online issue, which is available at www.interscience.wiley.com.]

slow increase and maximal enhancement during the portal phase or later. This suggests that preexisting hepatic arteries have decreased, portal veins are preserved, and neovascularized arteries are insufficient. In addition, we observed that those three nodules had cell change and the sinusoids were remarkably compressed, which would be another reason that the RE-T curve shows a slow increase in SI after Gd-DTPA injection.

To summarize, some LGDNs had the same blood supply as the surrounding cirrhotic liver and some were hypovascular. The HGDNs in our study were all hypovascular. Although most DNs are hypovascular lesions, a number of DNs appear different from the described principles. Matsui et al (13) found fewer hyperattenuating DNs with CTHA, which represents an increase in hepatic arterial supply, and Krinsky et al (29) found DNs with significantly increased arterial blood supply. However, in our study, we did not find hypervascular DNs, which may be due to the relatively small sample of DNs in our study. Nevertheless, there is no doubt that perfusion-weighted MRI can successfully reveal the blood supply of DNs.

Our study had some limitations. One limitation is that we could not evaluate the arterialization and capillarization of sinusoids, which takes place during the evolution from cirrhotic nodule to HCC. The enhancement of dynamic contrast-enhanced MRI is influenced by the extent and pattern of neovascularity, vessel permeability, cellularity, interstitial pressure, and fraction of extracellular space (30). Several studies (14,31,32) have reported the association of dynamic-enhancement MRI parameters with angiogenesis in HCCs and other malignant tumors. MR parameters, especially the RE and slope, showed a significant correlation with the degree of angiogenesis in tumors. Wang et al (31) found that the RE of dynamic-enhancement MRI of HCCs strongly correlates with tumor microvessel density, which is widely used to reflect the extent of sinusoidal capillarization in HCCs. There is also a correlation between dynamic MRI parameters and the expression of vascular endothelial growth factor (VEGF). However, Kanematsu et al (33,34) reported no correlation between dynamic-enhancement MRI parameters and the intensity of VEGF expression in HCC. Thus, the results of correlation studies on dynamic MRI and the VEGF expression are conflicting. One reason is the variability in methods of assessment and parameters employed in different studies. It is also likely that the current gold standard for assessing angiogenetic activity, VEGF expression, may not fully describe the functional angiogenetic status of the tumor. In addition to sinusoidal capillarization, it is well known that during the evolution from DN to HCC, there is a stepwise increase in unpaired arteries. Kim et al (22) observed that the degree of contrast enhancement of nodular HCCs in the arterial phase tended to correlate with the number of unpaired arteries. To our knowledge, no work has identified a correlation between contrast-enhanced MRI and unpaired arteries in HCCs and DNs. Therefore, further studies focusing on the correlation of perfusion-weighted MR parameters and specific pathological changes in vessels during the evolution from DN to HCC are required in the future.

Another limitation is that we only used semiquantitative parameters to monitor the blood supply of hepatic nodules. Considering that there is a change in blood supply from portal to arterial as a DN becomes an HCC, accurate quantification of arterial and portal venous perfusion of hepatic nodules would have great clinical value. van Laarhoven et al (35) described a method to calculate the kinetic parameters of dynamic MRI using a physiological pharmacokinetic model in the liver. However, the method can not be used to determine arterial and portal venous perfusion. CT perfusion imaging can determine the hepatic perfusion index including arterial and portal venous perfusion (16,36–38), but because many DNs and even some HCCs are isoattenuating with CT, the blood supply to the hepatic nodule would need to be investigated retrospectively by correlating radiologic and pathologic findings. It is very difficult to pinpoint the exact location of the original lesion in this retrospective fashion. Furthermore, the radiation dose during CT perfusion should also be considered. Unlike CT, the relationship between the concentration of gadolinium-based contrast agents and SI in MRI is nonlinear and complex. Thus, at present, accurate quantification in perfusion-weighted MRI (e.g., a dual-input single-compartment model for liver perfusion to estimate arterial and portal blood flow, distribution volume, and mean transit time in the liver of rabbits (15,39)) to evaluate perfusion parameters in humans is still challenging (40,41). For this technique to be clinically useful in the future, automated image processing tools that enable more accurate quantification of arterial and portal venous perfusion are needed.

Finally, owing to the 1.5T MR scanner and the limits of the sequence used, we could only apply single-slice perfusion-weighted MRI in one nodule at a time. With the advance of technical equipment and new sequence techniques (e.g., fast volume 3D imaging) as well as software, future efforts to establish whole-liver perfusion imaging as a clinically feasible and reliable technique may have profound implications for patients.

In conclusion, our study demonstrated that perfusion-weighted MRI can be applied successfully to evaluate the intranodular hemodynamic characteristics of DNs and HCCs in cirrhotic liver. Furthermore, it has the clinical potential to monitor blood supply changes of hepatic nodules in cirrhotic liver through repeated use in the same individual. However, further efforts to establish whole-liver perfusion imaging and accurate quantification of arterial and portal venous perfusion are needed to enable its wide clinical use.

ACKNOWLEDGMENT

We thank Mrs. Xue-Hui Yao for her assistance and invaluable help.

REFERENCES

1. Parkin DM. Global cancer statistics in the year 2000. Lancet Oncol 2001;2:533–543.
2. Unoura M, Kaneko S, Matsushita E, et al. High-risk groups and screening strategies for early detection of hepatocellular carcinoma in patients with chronic liver disease. Hepatogastroenterology 1993;40:305–310.
3. El-Serag HB, Mason AC. Rising incidence of hepatocellular carcinoma in the United States. N Engl J Med 1999;340:745–750.
4. Terminology of nodular hepatocellular lesions. International working party. Hepatology 1995;22:983–993.
5. Kojiro M. Focus on dysplastic nodules and early hepatocellular carcinoma: an Eastern point of view. Liver Transpl 2004;10(Suppl 1):S3–S8.
6. Kobayashi M, Ikeda K, Hosaka T, et al. Dysplastic nodules frequently develop into hepatocellular carcinoma in patients with chronic viral hepatitis and cirrhosis. Cancer 2006;106:636–647.
7. Efremidis SC, Hytiroglou P. The multistep process of hepatocarcinogenesis in cirrhosis with imaging correlation. Eur Radiol 2002; 12:753–764.
8. Taguchi K, Aishima S, Matsuura S, et al. Significance of the relationship between irregular regeneration and two hepatocarcinogenic pathways: "de novo" and so-called "dysplastic nodule-hepatocellular carcinoma" sequence. J Surg Oncol 2005;92:100–103.
9. van den Bos IC, Hussain SM, Terkivatan T, Zondervan PE, de Man RA. Stepwise carcinogenesis of hepatocellular carcinoma in the cirrhotic liver: demonstration on serial MR imaging. J Magn Reson Imaging 2006;24:1071–1080.
10. Sakamoto M, Hirohashi S, Shimosato Y. Early stages of multistep hepatocarcinogenesis: adenomatous hyperplasia and early hepatocellular carcinoma. Hum Pathol 1991;22:172–178.
11. Mazzaferro V, Regalia E, Doci R, et al. Liver transplantation for the treatment of small hepatocellular carcinomas in patients with cirrhosis. N Engl J Med 1996;334:693–699.
12. Hayashi M, Matsui O, Ueda K, Kawamori Y, Gabata T, Kadoya M. Progression to hypervascular hepatocellular carcinoma: correlation with intranodular blood supply evaluated with CT during intraarterial injection of contrast material. Radiology 2002;225:143–149.
13. Matsui O, Kadoya M, Kameyama T, et al. Benign and malignant nodules in cirrhotic livers: distinction based on blood supply. Radiology 1991;178:493–497.
14. Wang J, Chen LT, Tsang YM, Liu TW, Shih TT. Dynamic contrast-enhanced MRI analysis of perfusion changes in advanced hepatocellular carcinoma treated with an antiangiogenic agent: a preliminary study. AJR Am J Roentgenol 2004;183:713–719.
15. Guan S, Zhao WD, Zhou KR, et al. Sequential hemodynamic changes in precancerous lesions of hepatocellular carcinoma: experimental study with MR perfusion. Chin J Radiol 2006;40:231–234.
16. Fournier LS, Cuenod CA, de Bazelaire C, et al. Early modifications of hepatic perfusion measured by functional CT in a rat model of hepatocellular carcinoma using a blood pool contrast agent. Eur Radiol 2004;14:2125–2133.
17. Ha WS, Kim CK, Song SH, Kang CB. Study on mechanism of multistep hepatotumorigenesis in rat: development of hepatotumorigenesis. J Vet Sci 2001;2:53–58.
18. Zhao WD, Guan S, Zhou KR, et al. In vivo detection of metabolic changes by 1H-MRS in the DEN-induced hepatocellular carcinoma in Wistar rat. J Cancer Res Clin Oncol 2005;131:597–602.
19. Hayashi M, Matsui O, Ueda K, et al. Correlation between the blood supply and grade of malignancy of hepatocellular nodules associated with liver cirrhosis: evaluation by CT during intraarterial injection of contrast medium. AJR Am J Roentgenol 1999;172:969–976.
20. Ueda K, Terada T, Nakanuma Y, Matsui O. Vascular supply in adenomatous hyperplasia of the liver and hepatocellular carcinoma: a morphometric study. Hum Pathol 1992;23:619–626.
21. Park YN, Yang CP, Fernandez GJ, Cubukcu O, Thung SN, Theise ND. Neoangiogenesis and sinusoidal "capillarization" in dysplastic nodules of the liver. Am J Surg Pathol 1998;22:656–662.
22. Kim CK, Lim JH, Park CK, Choi D, Lim HK, Lee WJ. Neoangiogenesis and sinusoidal capillarization in hepatocellular carcinoma: correlation between dynamic CT and density of tumor microvessels. Radiology 2005;237:529–534.
23. Roncalli M, Roz E, Coggi G, et al. The vascular profile of regenerative and dysplastic nodules of the cirrhotic liver: implications for diagnosis and classification. Hepatology 1999;30:1174–1178.
24. Vogl TJ, Stupavsky A, Pegios W, et al. Hepatocellular carcinoma: evaluation with dynamic and static gadobenate dimeglumine-enhanced MR imaging and histopathologic correlation. Radiology 1997;205:721–728.

25. Yamashita Y, Fan ZM, Yamamoto H, et al. Spin-echo and dynamic gadolinium-enhanced FLASH MR imaging of hepatocellular carcinoma: correlation with histopathologic findings. J Magn Reson Imaging 1994;4:83–90.
26. Lim JH, Cho JM, Kim EY, Park CK. Dysplastic nodules in liver cirrhosis: evaluation of hemodynamics with CT during arterial portography and CT hepatic arteriography. Radiology 2000;214:869–874.
27. Tajima T, Honda H, Taguchi K, et al. Sequential hemodynamic change in hepatocellular carcinoma and dysplastic nodules: CT angiography and pathologic correlation. AJR Am J Roentgenol 2002;178:885–897.
28. Nakashima Y, Nakashima O, Hsia CC, Kojiro M, Tabor E. Vascularization of small hepatocellular carcinomas: correlation with differentiation. Liver 1999;19:12–18.
29. Krinsky GA, Theise ND, Rofsky NM, Mizrachi H, Tepperman LW, Weinreb JC. Dysplastic nodules in cirrhotic liver: arterial phase enhancement at CT and MR imaging—a case report. Radiology 1998;209:461–464.
30. Kuhl CK, Schild HH. Dynamic image interpretation of MRI of the breast. J Magn Reson Imaging 2000;12:965–974.
31. Wang B, Gao ZQ, Yan X. Correlative study of angiogenesis and dynamic contrast-enhanced magnetic resonance imaging features of hepatocellular carcinoma. Acta Radiol 2005;46:353–358.
32. Buadu LD, Murakami J, Murayama S, et al. Breast lesions: correlation of contrast medium enhancement patterns on MR images with histopathologic findings and tumor angiogenesis. Radiology 1996;200:639–649.
33. Kanematsu M, Osada S, Amaoka N, et al. Expression of vascular endothelial growth factor in hepatocellular carcinoma and the surrounding liver and correlation with MRI findings. AJR Am J Roentgenol 2005;184:832–841.
34. Kanematsu M, Semelka RC, Leonardou P, et al. Angiogenesis in hepatocellular nodules: correlation of MR imaging and vascular endothelial growth factor. J Magn Reson Imaging 2004;20:426–434.
35. van Laarhoven HW, Rijpkema M, Punt CJ, et al. Method for quantitation of dynamic MRI contrast agent uptake in colorectal liver metastases. J Magn Reson Imaging 2003;18:315–320.
36. Miles KA, Leggett DA, Kelley BB, Hayball MP, Sinnatamby R, Bunce I. In vivo assessment of neovascularization of liver metastases using perfusion CT. Br J Radiol 1998;71:276–281.
37. Tsushima Y, Funabasama S, Aoki J, Sanada S, Endo K. Quantitative perfusion map of malignant liver tumors, created from dynamic computed tomography data. Acad Radiol 2004;11:215–223.
38. Van Beers BE, Leconte I, Materne R, Smith AM, Jamart J, Horsmans Y. Hepatic perfusion parameters in chronic liver disease: dynamic CT measurements correlated with disease severity. AJR Am J Roentgenol 2001;176:667–673.
39. Van Beers BE, Materne R, Annet L, et al. Capillarization of the sinusoids in liver fibrosis: noninvasive assessment with contrast-enhanced MRI in the rabbit. Magn Reson Med 2003;49:692–699.
40. Pandharipande PV, Krinsky GA, Rusinek H, Lee VS. Perfusion imaging of the liver: current challenges and future goals. Radiology 2005;234:661–673.
41. Materne R, Smith AM, Peeters F, et al. Assessment of hepatic perfusion parameters with dynamic MRI. Magn Reson Med 2002; 47:135–142.